Supporting Information

Efficient Electrocatalytic Nitric Oxide Reduction to Ammonia by Manganese Spinel Oxides

Zhaodong Niu[a], Shiying Fan[a], Xinyong Li[a,*]

[a]*State Key Laboratory of Fine Chemicals, Key Laboratory of Industrial Ecology and Environmental Engineering (MOE), School of Environmental Science and Technology, Dalian University of Technology, Dalian 116024, PR China*

Experimental Methods

Prepared of catalysts

The precursor fibers were prepared according to a previously reported method with some modifications.[1] Typically, Polyacrylonitrile (PAN, Mw = 150,000) and polystyrene (PS) were dispersed into 10 mL of N,N'-Dimethylformamide (DMF, 99.5%) with magnetic stirring at 60 °C for 8 h to obtain a uniform solution. Subsequent, a certain amount of manganese acetate ($Mn(CH_3COO)_2 \cdot 4H_2O$, 99%) and $M(CH_3COO)_2 \cdot xH_2O$ (M = Co, Ni and Zn) were added to the above solution with vigorous stirring at room temperature overnight. Then, the precursor fibers were obtained by electrospinning with voltage, feeding rate and distance (between the collector and the needle) of 17 kV, 1 mL h^{-1} and 15 cm. Finally, the as-prepared fibers were stabilized in a muffle furnace at 200 °C for 2 h with 2 °C min^{-1} to obtain MMn/PAN&PS (M = Co, Ni and Zn). The CoMn/PAN&PS fibers were annealed at 800 °C for 3 h with 2 °C min^{-1} under a N_2 flow, and then the material was transferred to muffle furnace at 300 °C for 3 h with 2 °C min^{-1} to obtain $CoMn_2O_4$/C. The MMn/PAN&PS (M = Co, Ni and Zn) fibers were calcined in a muffle furnace at 600 °C for 2 h with 2 °C min^{-1} to obtain $CoMn_2O_4$ (M = Co, Ni and Zn). The pure PC fibers were prepared similar to $CoMn_2O_4$/C and without metal salt.

Material characterizations

X-ray diffraction (XRD) patterns were carried out on Bruker D8 Advance with a Cu Kα radiation. Scanning transmission microscope (SEM) conducted under FEI (Nova Nano SEM 450). Transmission electron microscope (TEM) was measured using JEOL (JEM F200) with an energy-dispersive X-ray spectroscopy (EDX) detector. X-ray photoelectron spectroscopy (XPS) was carried out using an X-ray photoelectron spectrometer (Thermos K-Alpha+) with Al Kα as the X-ray source.

Electrochemical measurements

All electrochemical measurements were performed on a CHI 660E electrochemical workstation (Shanghai Chenhua, China) at room temperature. A homemade three-electrode two-compartment H-cell was used with a separate membrane of Nafion 117 (Dupont). Before use, the membrane was pretreated sequentially in 5 wt% H_2O_2, 1 M H_2SO_4 and water at 80 ℃ for 1 h. A piece of carbon cloth (1 × 1 cm^2) loaded with catalyst, Ag/AgCl (saturated KCl solution) and Pt plate (1 × 1.5 cm^2) were used as the working electrode, reference electrode and counter electrode, respectively. Typically, 10 mg of catalyst was dispersed in 720 μL of ethanol, 240 μL of water and 40 μL of Nafion (5 wt%, Dupont) with sonication for 1 h to form a homogenous ink. The prepared catalyst ink was drop-cast onto the carbon cloth (HCP330N, Hesen Co., Ltd.) (40 μL, 1 × 1 cm^2) and dried at room temperature to obtain the working electrode (0.4 mg cm^{-2}). The electrolyte of the anode and cathode was 0.1 M sodium sulphate (Na_2SO_4, 99%) (40 mL). The electrolyte was pre-saturated with Ar (99.999%, 30 mL min^{-1}) by bubbling for at least 30 min before electrolysis. For NORR, NO (99.9vol% or 20vol% NO/Ar, 30 mL min^{-1}) saturated 0.1 M Na_2SO_4 was used as the catholyte. Linear sweep voltammetry (LSV) curve was measured with a scan rate of 50 mV s^{-1}. All potentials were converted based on the Nernst equation of $E_{RHE} = E_{Ag/AgCl} + 0.0591 \times pH + 0.197$.

Ammonia detection and calculation method

The NH_3 concentration was detected by the indophenol blue method.[2, 3] Typical, 1 mL of diluted electrolyte was mixed with 1 mL of 1 M sodium hydroxide (NaOH, 96%) solution containing 5 wt% salicylic acid (99%) and 5 wt% sodium citrate dihydrate (99%). Then, 0.5 mL of 0.05 M sodium hypochlorite (NaClO, 6 ~ 14% active chlorine basis) and 0.1 mL of sodium nitroferric cyanide ($C_5FeN_6Na_2O$, 99%) (1 wt%) were added to the above solution. After standing for 2 h at ambient conditions, the absorption spectrum was recorded by using a UV-vis

spectrophotometer at 654 nm. The ^{1}H nuclear magnetic resonance (^{1}H-NMR) was measured by using Bruker 400 MHz. The pH of the electrolyte was adjusted to about 2.0 by adding 4 M H_2SO_4. The deuterium oxide (D_2O) and maleic acid (MA, 99%) were used as the deuterium reagent and internal standard, respectively. The Faradaic efficiency and yield rate were calculated by the following equation:

$$\text{Faradaic efficiency} = (nF \times c \times V)/(M \times Q)$$

$$\text{Yield rate} = (c \times V)/(M \times t \times m)$$

where n is the number of electrons transferred, F is the Faradaic constant (96,485 C mol^{-1}), c is the concentration of products, V is the volume of catholyte (0.04 L), M is the relative molecular mass, Q is the total charge (C), t is the electroreduction time (1 h), and m is the mass of the catalyst on the cathode (g).

In situ Raman spectroscopy measurements

In situ Raman spectroscopy measurements were performed on a Renishaw inVia Qontor Raman Microscope system with a homemade three-electrode H-cell (Nafion 117 membrane) at room temperature. The graphite rod and Ag/AgCl electrode (saturated KCl solution) were used as the counter and reference electrode, respectively. A piece of carbon paper (1.5 × 1.5 cm^2) was used as the substrate of the catalysts to prepare the working electrode. The catholyte was 0.1 M Na_2SO_4 saturated with Ar or NO (99.9vol%), respectively. The electrode potentials were set with reference to NORR electrolysis experiments (−0.5 ~ −0.8 V vs. RHE). A long focal length distance objective (Leica, 50×) was used for focusing. The wavelength of the excitation source of the laser is 532 nm with an intensity of 10%.

Density functional theory calculations

Density functional theory (DFT) were carried out to calculate the conversion of NO into NH_3 on catalysts by using the Vienna *ab initio* simulation package (VASP) code.[4, 5] The projector augmented wave (PAW) approach was adopted to describe the

ion-electron interaction.[6] The cut-off energy and energy convergence were set to 400 eV and 1×10^{-5} eV, respectively. The generalized gradient approximation (GGA) with the Perdew-Burke-Ernzerhof (PBE) functional was used to describe the electron exchange and correlation energy.[7] Brillouin zone integration was accomplished using a 4 × 4 × 1 Monkhorst-Pack k-point mesh. A vacuum space with 15 Å was inserted in the z-direction. The chemical potential of a proton-electron pair ($\mu(H^+) + \mu(e^-)$) is equal to the half of the chemical potential of one gaseous hydrogen ($1/2\mu(H_2)$). The Gibbs free energies of the reaction were calculated as follows equation (U = 0 V):

$$\Delta G = \Delta E + \Delta E_{ZPE} - T\Delta S$$

where ΔE is the reaction energy difference between the products and reactants; ΔE_{ZPE} is the change of zero-point energy; ΔS and T (298 K) is entropy change and temperature, respectively.

Results and Discussion

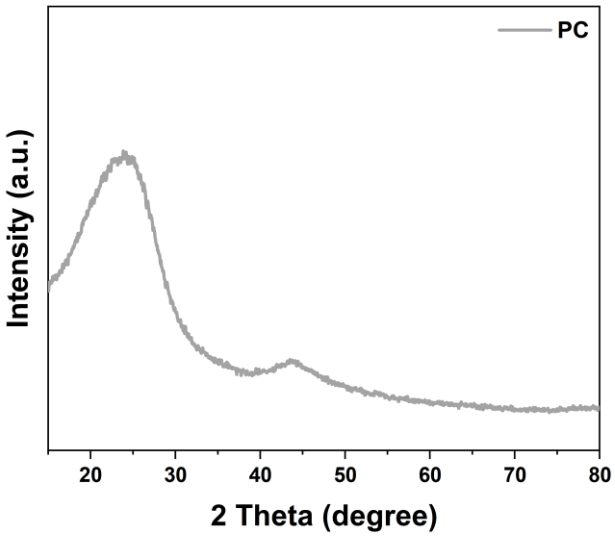

Fig. S1. XRD pattern of PC.

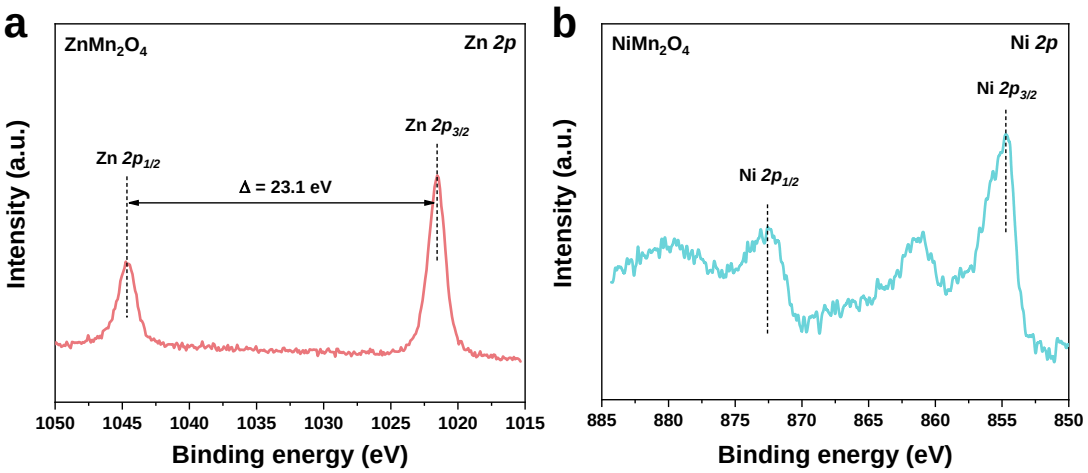

Fig. S2. XPS (a) Zn 2p and (b) Ni 2p spectra of $ZnMn_2O_4$ and $NiMn_2O_4$.

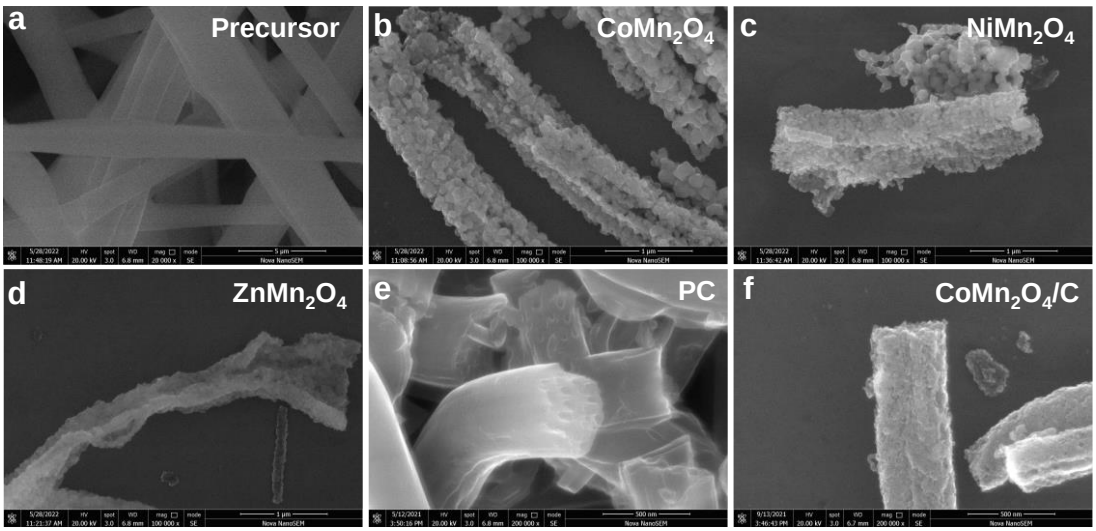

Fig. S3. SEM images of (a) precursor fibers, (b) $CoMn_2O_4$, (c) $NiMn_2O_4$, (d) $ZnMn_2O_4$, (e) PC and (f) $CoMn_2O_4$/C.

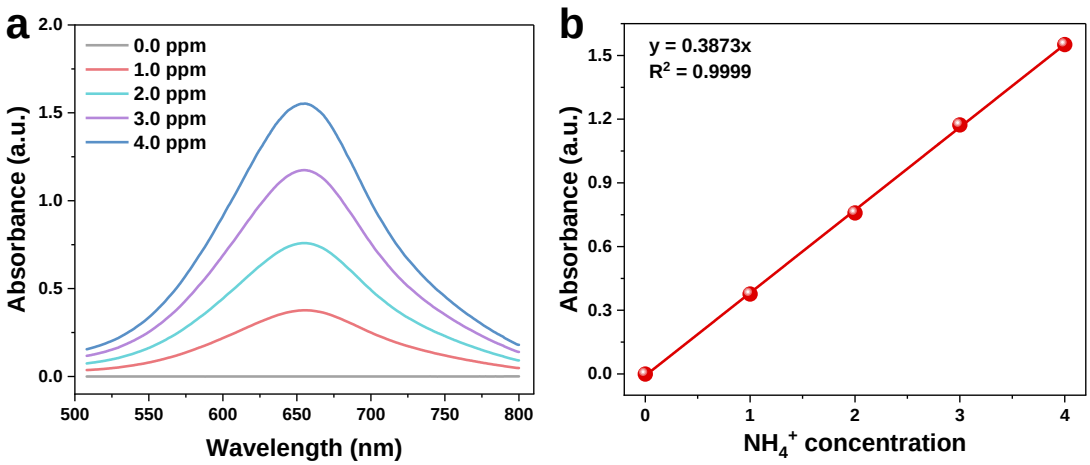

Fig. S4. (a) UV-vis absorption spectra of NH_3 solution with different concentrations and (b) corresponding calibration curves.

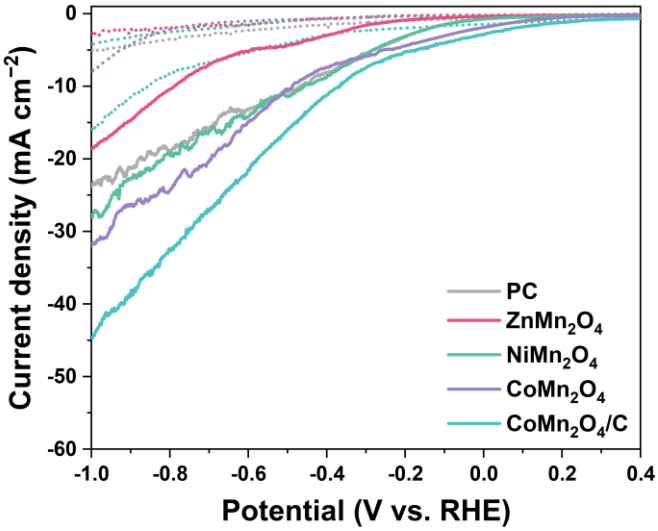

Fig. S5. LSV curves of CP, MMn_2O_4 (M = Zn, Ni and Co) and $CoMn_2O_4$/C in Ar (short dot) and 99.9vol% NO (solid) saturated 0.1 M Na_2SO_4 in H-type cell.

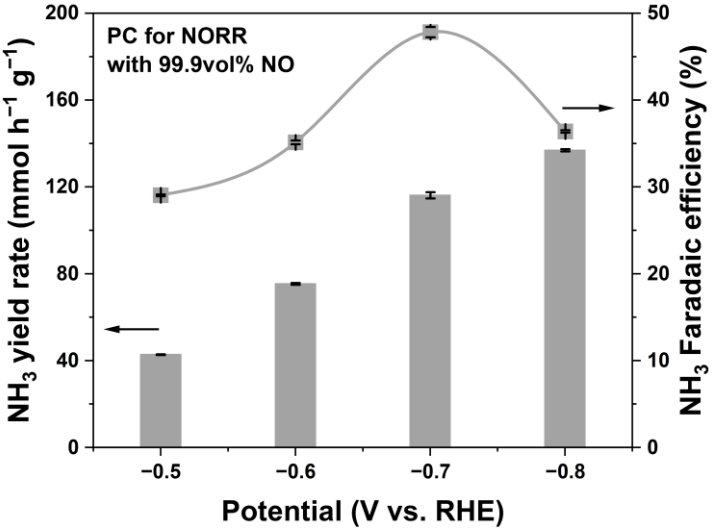

Fig. S6. NH_3 yield rate and Faradaic efficiency of $CoMn_2O_4$/C at different potentials in 20vol% NO saturated 0.1 M Na_2SO_4.

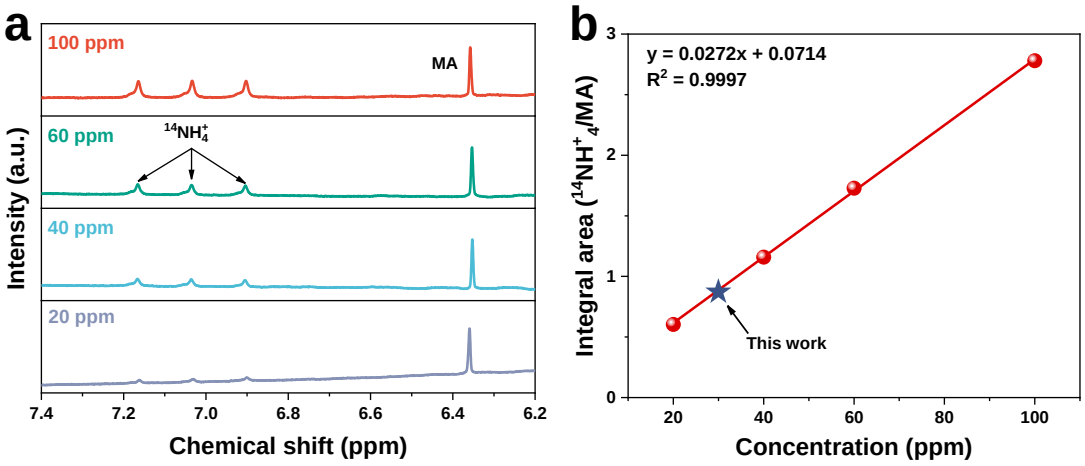

Fig. S7. (a) ^{1}H-NMR calibration curve of NH_3 using $^{14}NH_4Cl$ solutions of known concentration (NH_4^+) as standards and (b) corresponding calibration curves.

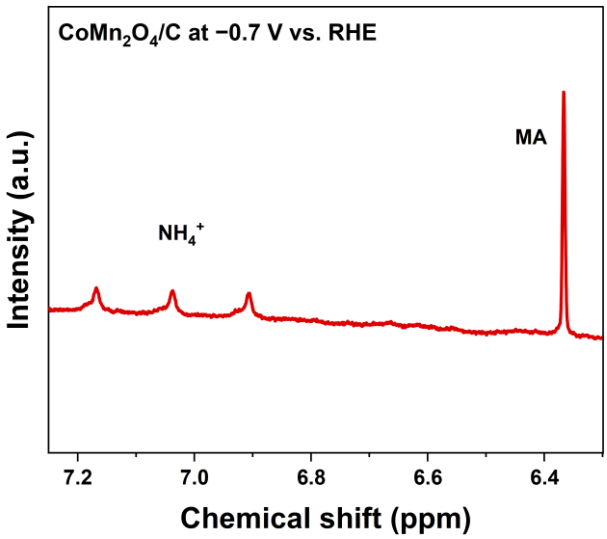

Fig. S8. ^{1}H-NMR spectra for the electrolyte after ^{14}NORR at −0.7 V vs. RHE for 20 min in 99.9vol% NO saturated 0.1 M Na_2SO_4.

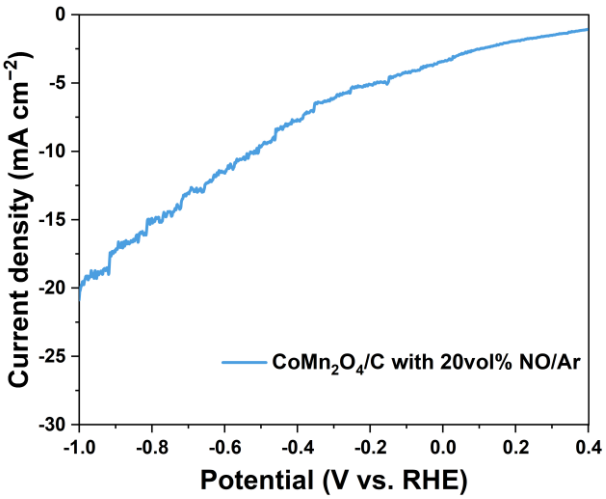

Fig. S9 LSV curves of $CoMn_2O_4$/C in 20vol% NO saturated 0.1 M Na_2SO_4 in H-type cell.

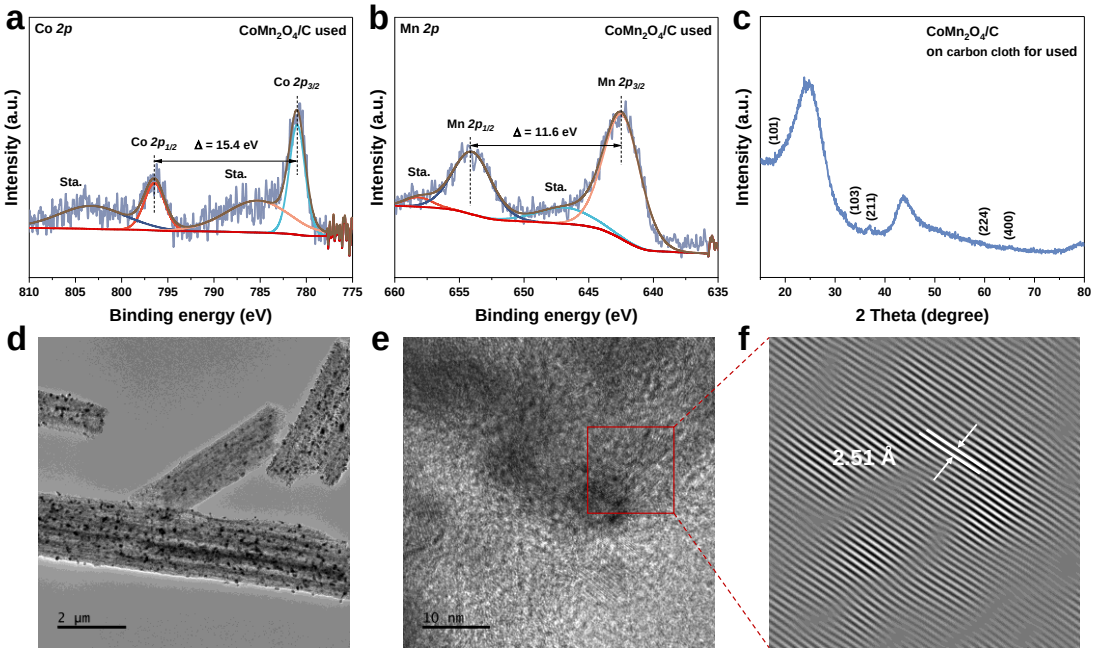

Fig. S10. High-resolution XPS spectra of (a) Co *2p* and (b) Mn *2p*, (c) XRD pattern, (d) TEM, (e) HRTEM and (f) IFFT images of $CoMn_2O_4$/C after NORR.

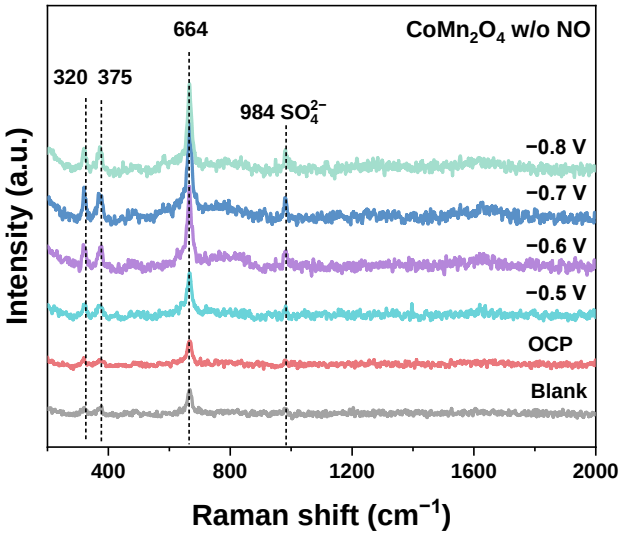

Fig. S11. *In situ* Raman spectra of $CoMn_2O_4$ in 0.1 M Na_2SO_4 without NO at different potentials.

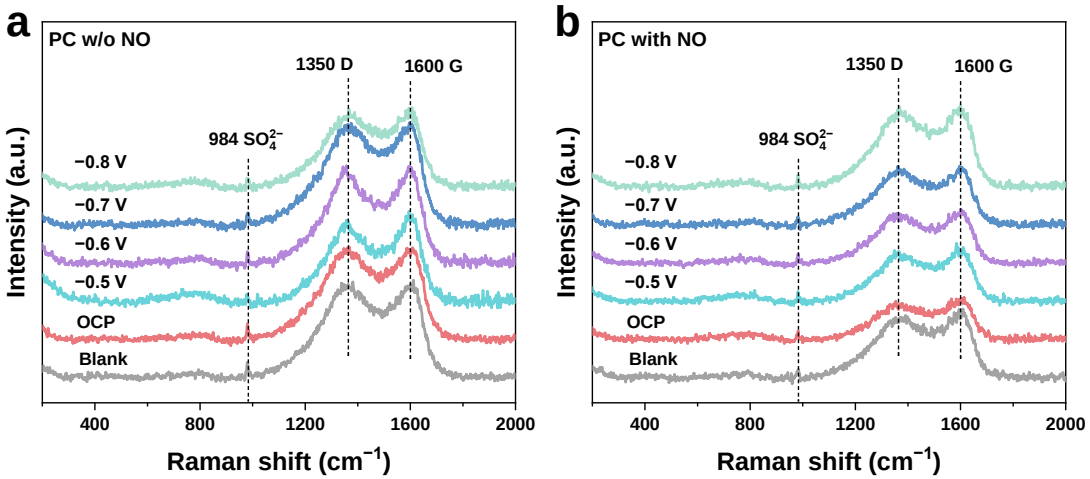

Fig. S12. *In situ* Raman spectra of PC in 0.1 M Na_2SO_4 with and without NO at different potentials.

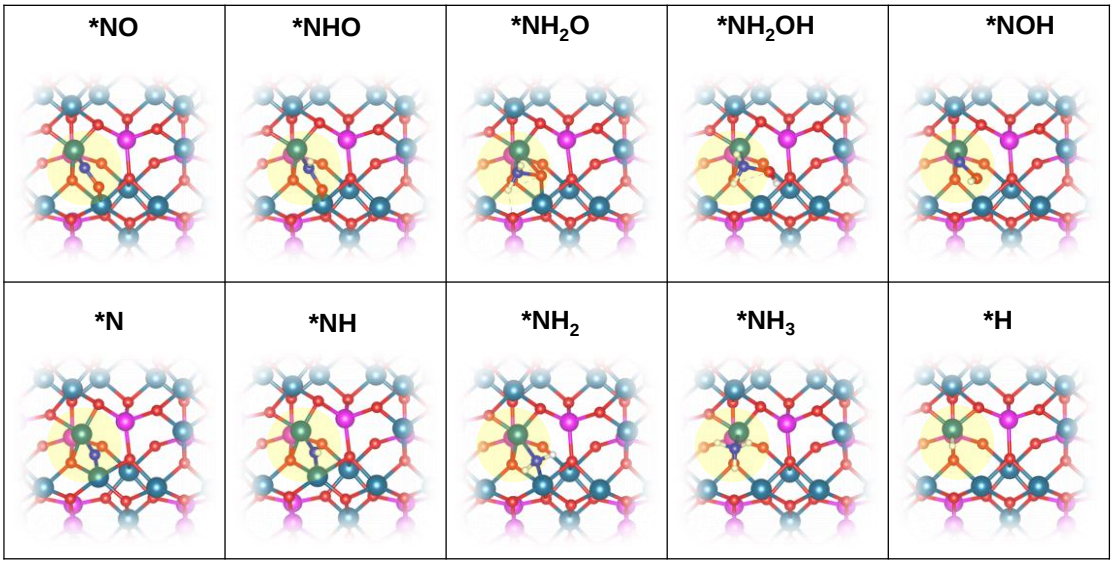

Fig. S13. Optimized geometric structure of intermediates adsorbed on the substrate of $CoMn_2O_4$ for NORR. The green, pink, blue, red and white balls refer to Mn, Co, N, O and H atoms.

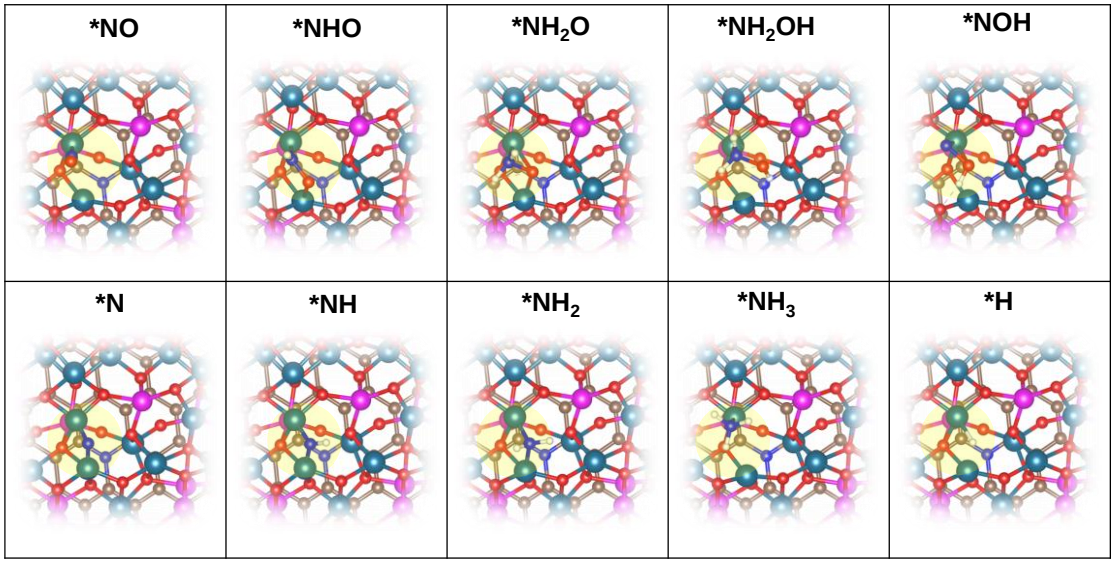

Fig. S14. Optimized geometric structure of intermediates adsorbed on the substrate of $CoMn_2O_4$/C for NORR. The green, pink, blue, golden, red and white balls refer to Mn, Co, N, C, O and H atoms.

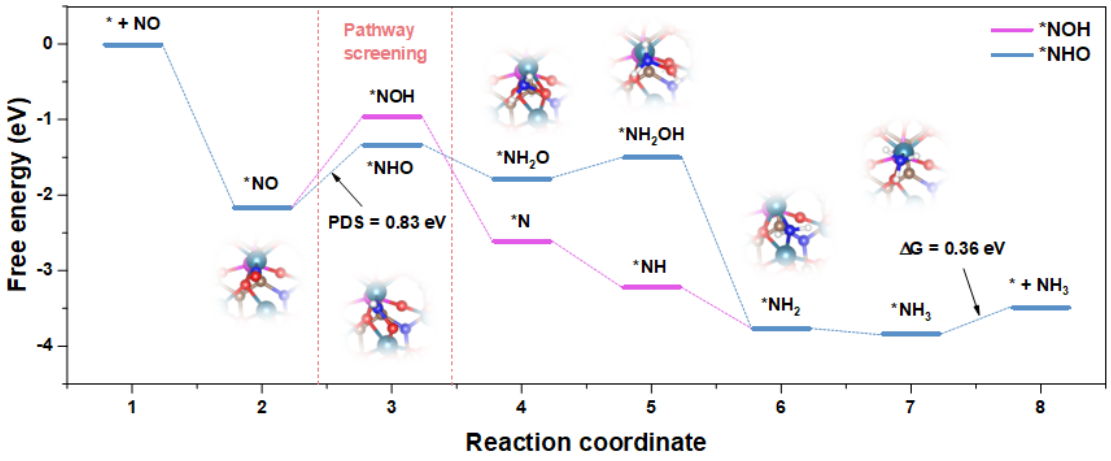

Fig. S15. Free energy diagram of NORR to NH_3 over $CoMn_2O_4$/C (U = 0 V vs. RHE).

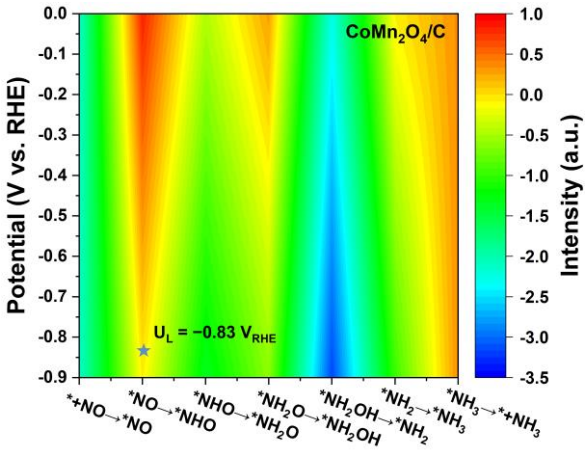

Fig. S16. Contour maps of free energy changes of elementary steps at different potentials for $CoMn_2O_4$/C.

Table S1 Performance comparison with other metal-based catalysts for NO electrochemical reduction into NH_3 (H-type cell).

Catalysts	NH_3 yield rate	Faradaic efficiency (%)	Conditions	Ref.
$CoMn_2O_4$/C	497.6 mmol h^{-1} g^{-1} (199.0 μmol h^{-1} cm^{-2})	89.3	0.1 M Na_2SO_4, 99.9vol% NO, −0.7 V vs. RHE	**This work**
	203.2 mmol h^{-1} g^{-1} (81.3 μmol h^{-1} cm^{-2})	85.0	0.1 M Na_2SO_4, 20vol% NO/Ar, −0.7 V vs. RHE	
$CoMn_2O_4$	325.0 mmol h^{-1} g^{-1} (130.0 μmol h^{-1} cm^{-2})	86.3	0.1 M Na_2SO_4, 99.9vol% NO, −0.7 V vs. RHE	
Cu foam	9.234 mmol h^{-1} g^{-1} (517.1 μmol h^{-1} cm^{-2})	93.5	0.25 Li_2SO_4, 99.9vol% NO, −0.9 V vs. RHE	8
Fe_2O_3/CP	13.0 mmol h^{-1} g^{-1} (~46 μmol h^{-1} cm^{-2})	86.7	0.1 M Na_2SO_4 + 0.05 mM Fe^{2+}EDTA, 99.9vol% NO, −0.4 V vs. RHE	9
Cu_2O@$CoMn_2O_4$	94.2 mmol h^{-1} g^{-1}	75.1	0.1 M Na_2SO_4, 99.9vol% NO, −0.9 V vs. RHE	10
Nb-SA/BNC	494 mmol h^{-1} g^{-1}	77	0.1 M HCl, 99.9vol% NO, −0.6 V vs. RHE	11
Co_1/MoS_2	435.2 mmol h^{-1} g^{-1} (217.6 μmol h^{-1} cm^{-2})	87.7	0.5 M Na_2SO_4, 99.9vol% NO, −0.5 V vs. RHE	12
CuFe DS/NC	187.5 mmol h^{-1} g^{-1} (112.52 μmol h^{-1} cm^{-2})	90	0.1 M Na_2SO_4, 99.9vol% NO, −0.6 V vs. RHE	13
bcc RuGa IMCs	320.6 mmol h^{-1} g^{-1}_{Ru}	72.3	0.1 M K_2SO_4, 20vol% NO/Ar, −0.2 V vs. RHE	14
Bi NDs/CP	70.2 mmol h^{-1} g^{-1}	89.2	0.1 M Na_2SO_4 + 0.05 mM Fe^{2+}EDTA, 10vol% NO/Ar, −0.6 V vs. RHE	15
MoS_2/GF	~3.3 mmol h^{-1} g^{-1} (~20 μmol h^{-1} cm^{-2})	76.6	0.1 M HCl + 0.5 mM Fe^{2+}SB, 10vol% NO/Ar, 0.1 V vs. RHE	16
Ru-LCN	45.02 mmol h^{-1} g^{-1}	65.96	0.5 M Na_2SO_4, 1vol% NO/Ar, 0.1 V vs. RHE	17

References

1. S. Liu; X. F. Lu; J. Xiao; X. Wang; X. W. D. Lou, *Angew. Chem. Int. Ed.* 2019, **58**, 13828-13833.
2. Z. Niu; S. Fan; X. Li; Z. Liu; J. Wang; J. Duan; M. O. Tade; S. Liu, *ACS Appl. Mater. Interfaces* 2022, **14**, 35477-35484.
3. F.-Y. Chen; Z.-Y. Wu; S. Gupta; D. J. Rivera; S. V. Lambeets; S. Pecaut; J. Y. T. Kim; P. Zhu; Y. Z. Finfrock; D. M. Meira; G. King; G. Gao; W. Xu; D. A. Cullen; H. Zhou; Y. Han; D. E. Perea; C. L. Muhich; H. Wang, *Nat. Nanotechnol.* 2022, **17**, 759-767.
4. J. Hafner, *Computational Chemistry* 2008, **29**, 2044-2078.
5. G. K. A; J. F. b, *Computational Materials Science* 1996, **6**, 15-50.
6. P. E. Blochl, *Physical Review B* 1994, **50**, 17953-17979.
7. John; P.; Perdew; Kieron; Burke; Matthias; Ernzerhof; Erratum, *Phys. Rev. Lett.* 1996, **77**, 3865-3868.
8. J. Long; S. Chen; Y. Zhang; C. Guo; X. Fu; D. Deng; J. Xiao, *Angew. Chem. Int. Ed.* 2020, **59**, 9711-9718.
9. J. Liang; H. Chen; T. Mou; L. Zhang; Y. Lin; L. Yue; Y. Luo; Q. Liu; N. Li; A. A. Alshehri; I. Shakir; P. O. Agboola; Y. Wang; B. Tang; D. Ma; X. Sun, *J. Mater. Chem. A* 2022, **10**, 6454-6462.
10. C. Bai; S. Fan; X. Li; Z. Niu; J. Wang; Z. Liu; D. Zhang, *Adv. Funct. Mater.* 2022, 2205569.
11. X. Peng; Y. Mi; H. Bao; Y. Liu; D. Qi; Y. Qiu; L. Zhuo; S. Zhao; J. Sun; X. Tang; J. Luo; X. Liu, *Nano Energy* 2020, **78**, 105321.
12. X. Li; K. Chen; X. Lu; D. Ma; K. Chu, *Chem. Eng. J.* 2023, **454**, 140333.
13. D. Wang; X. Zhu; X. Tu; X. Zhang; C. Chen; X. Wei; Y. Li; S. Wang, *Adv. Mater.* 2023, e2304646.

14. H. Zhang; Y. Li; C. Cheng; J. Zhou; P. Yin; H. Wu; Z. Liang; J. Zhang; Q. Yun; A. L. Wang; L. Zhu; B. Zhang; W. Cao; X. Meng; J. Xia; Y. Yu; Q. Lu, *Angew. Chem. Int. Ed. Engl.* 2022, 202213351.
15. Y. Lin; J. Liang; H. Li; L. Zhang; T. Mou; T. Li; L. Yue; Y. Ji; Q. Liu; Y. Luo; N. Li; B. Tang; Q. Wu; M. S. Hamdy; D. Ma; X. Sun, *Mater. Today Phys.* 2022, **22**, 100611.
16. L. Zhang; J. Liang; Y. Wang; T. Mou; Y. Lin; L. Yue; T. Li; Q. Liu; Y. Luo; N. Li; B. Tang; Y. Liu; S. Gao; A. A. Alshehri; X. Guo; D. Ma; X. Sun, *Angew. Chem. Int. Ed.* 2021, **60**, 25263-25268.
17. Y. Li; C. Cheng; S. Han; Y. Huang; X. Du; B. Zhang; Y. Yu, *ACS Energy Lett.* 2022, **7**, 1187–1194.